

AMPA Receptors Regulate Exocytosis and Insulin Release in Pancreatic β Cells

Zhen-Yong Wu¹, Li-Jun Zhu¹, Na Zou¹, Lidija K. Bombek², Chong-Yu Shao¹, Na Wang¹, Xin-Xin Wang¹, Li Liang⁴, Jun Xia^{1,3}, Marjan Rupnik^{2,*} and Ying Shen^{1,*}

¹Department of Neurobiology, Key Laboratory of Medical Neurobiology of Ministry of Health, Zhejiang Province Key Laboratory of Neurobiology, Zhejiang University School of Medicine, Hangzhou, Zhejiang 310058, P. R. China

²Institute of Physiology, Faculty of Medicine, University of Maribor, Slomškova trg 15, 2000, Maribor, Slovenia

³Department of Biochemistry, Hong Kong University of Science and Technology, Clear Water Bay, Kowloon, Hong Kong, P. R. China

⁴Department of Endocrinology, Zhejiang Key Laboratory for Diagnosis and Therapy of Neonatal Diseases, Children's Hospital, Zhejiang University School of Medicine, Hangzhou, P. R. China

*Corresponding authors: Ying Shen, yshen@zju.edu.cn and Marjan Rupnik, marjan.rupnik@uni.mb.si

Ionotropic glutamate receptors (iGluRs) are expressed in islets and insulinoma cells and involved in insulin secretion. However, the exact roles that iGluRs play in β cells remain unclear. Here, we demonstrated that GluR2-containing α -amino-3-hydroxy-5-methyl-4-isoxazolepropionic acid receptors (AMPA receptors) were expressed in mouse β cells. Glutamate application increased both cytosolic calcium and the number of docked insulin-containing granules, which resulted in augmentation of depolarization-induced exocytosis and high-glucose-stimulated insulin release. While glutamate application directly depolarized β cells, it also induced an enormous depolarization when K_{ATP} channels were available. Glutamate application reduced the conductance of K_{ATP} channels and increased voltage oscillations. Moreover, actions of AMPARs were absent in Kir6.2 knock-out mice. The effects of AMPARs on K_{ATP} channels were mediated by cytosolic cGMP. Taken together, our experiments uncovered a novel mechanism by which AMPARs participate in insulin release.

Key words: β cell, AMPA receptor, cGMP, exocytosis, insulin, K_{ATP} channel

Received 25 November 2011, revised and accepted for publication 25 April 2012, uncorrected manuscript published online 27 April 2012

Insulin, stored in secretory granules of pancreatic β cells, is the major hormone-regulating glucose metabolism by complex but highly ordered mechanisms (1). The classic pathway for insulin release is that when the blood glucose level increases, glucose enters β cells through

glucose transporter subtype 2 and changes the ATP level. Increased ATP inhibits the ATP-sensitive potassium (K_{ATP}) channels and results in membrane depolarization and activation of voltage-gated calcium channels (VGCCs) (2,3). Thus, K_{ATP} channels play important roles in regulating insulin release.

Glutamate, the major excitatory neurotransmitter in the central nervous system, is found in pancreatic islets (4–6) and is released from α cells (7,8). Various ionotropic glutamate receptors (iGluRs) are found in insulinoma cells and islets (5,6). Some evidence shows that iGluRs are expressed in β cells and may modulate the level of insulin release (4–6,9,10). However, recent studies showed that functional iGluRs are expressed in α cells, but not in β cells (11,12). Therefore, the expression and roles of iGluRs in β cells need to be further explored.

In the present work, we used several techniques, including whole-cell patch-clamp recording in acute pancreatic tissue slices, single cell RT-PCR, immunohistochemistry and total internal reflection fluorescence microscopy (TIRFM) to investigate the functions of iGluRs in β cells. Our results demonstrated that functional GluR2-containing AMPARs were expressed in mouse β cells. AMPAR activation increased cytosolic cGMP and inhibited K_{ATP} channels, which in turn increased the intracellular calcium $[Ca^{2+}]_i$ and promoted the docking of insulin-containing granules. Therefore, exocytosis and insulin release were increased when a high driving force (depolarization or high glucose stimulation) occurred.

Results

Functional AMPARs are expressed in mouse β cells

We made whole-cell patch clamp recordings in mouse pancreatic slices to study iGluR-mediated currents in β cells. β cells were easily distinguished from α cells by its electrophysiological properties and insulin-specific expression (3,13). In voltage-clamp whole-cell mode, β cells exhibited a mean capacitance of 7.2 ± 0.6 pF ($n = 433$; $N = 109$), much bigger than non- β cells (14,15). When a stepped voltage stimulation protocol was given, voltage-gated Na^+ currents at hyperpolarizing potential and gap junction currents were present in β cells (Figure 1A1). Differently, voltage-gated Na^+ currents were present at resting potential and there were no gap junction currents in α cells (Figure 1B1). These results were consistent with previous reports (3,14,15). Moreover, β cells showed voltage oscillations in 11 mM glucose but no response in 0 glucose (Figure 1A2). α cells fired action potentials in 0 glucose but no

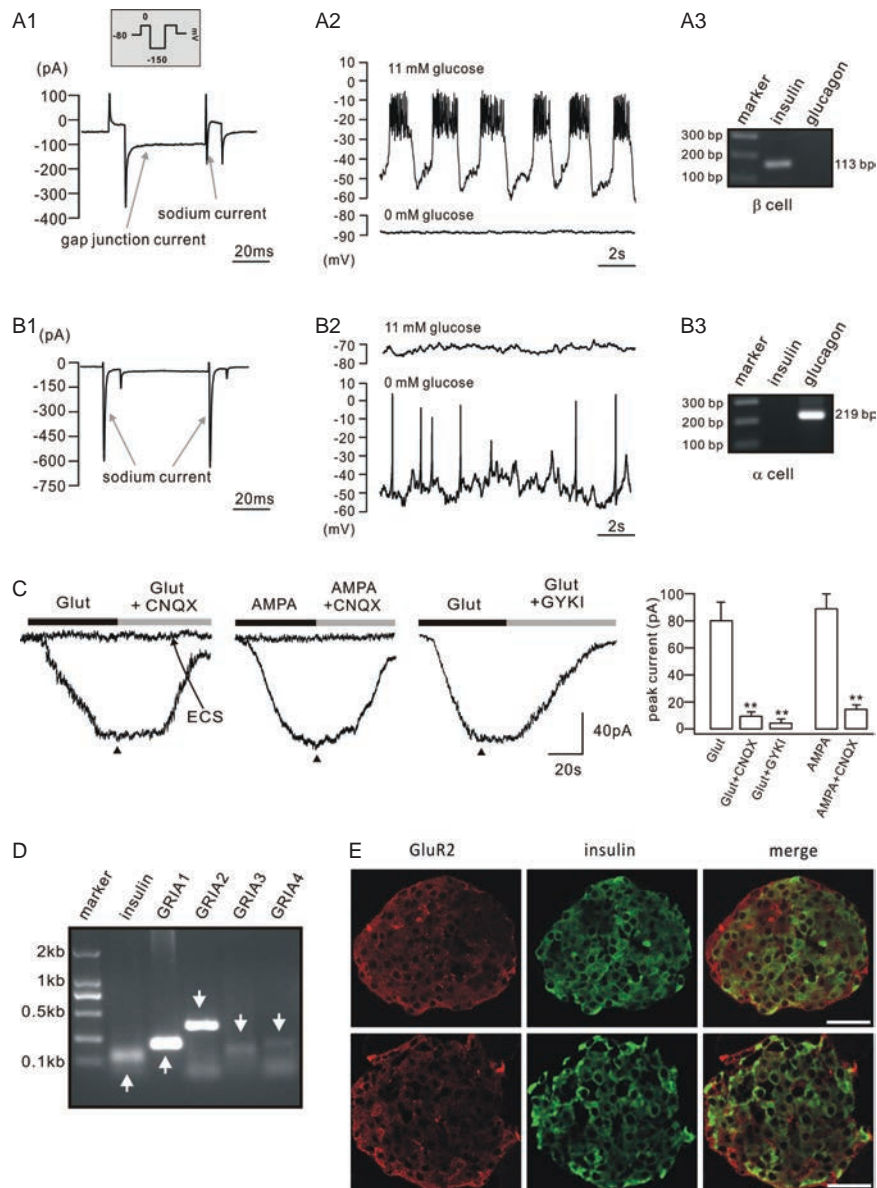


Figure 1: Expression of AMPARs in mouse β cells. A) Characterizations of β cells. A1 shows the representative voltage-gated sodium current from a β cell. There was one Na^+ spike at hyperpolarized holding potential ($n=433$; $N=109$). Another characteristic response was that a steady inward current occurred during a hyperpolarizing command ($n=433$; $N=109$), consistent with previous work (16). Inset at top illustrates the stepped voltage stimulation protocol. A2 shows representative voltage oscillations derived from a β cell that was challenged by 11 mM glucose in current-clamp configuration (upper panel; $n=40$; $N=30$), which did not occur in 0 mM glucose (low panel; $n=35$; $N=30$), consistent with previous work (16,17). A3 shows the ethidium bromide (EB)-stained gel from nested RT-PCR amplification of insulin from β cell ($n=40$; $N=30$). B) Characterizations of α cell. B1 shows the representative voltage-gated sodium current from an α cell. Two Na^+ spikes corresponded to the rise and the fall of the voltage step ($n=36$; $N=30$). There was no steady inward current during a hyperpolarizing command. B2 shows representative action potentials derived from an α cell that was challenged by 0 mM glucose in current-clamp configuration (low panel; $n=15$; $N=5$), which did not occur in 11 mM glucose (upper panel; $n=10$; $N=5$). B3 shows the EB gel from nested RT-PCR amplification of glucagon from α cell ($n=15$; $N=5$). C) Representative whole-cell currents induced by local application of glutamate (Glut) and AMPA. Traces indicated by the arrows (ECS) show recordings in the absence of agonists. Drug application is illustrated as black and gray bars above the traces. Filled triangles indicate the time points where peak currents were calculated. Upon application of CNQX or GYKI53655, remaining currents were 11 ± 1 pA (glutamate+CNQX, $n=46$; $N=16$), 4.1 ± 1.2 pA (glutamate+GYKI53655, $n=10$, $N=2$) and 10 ± 1 pA (AMPA+CNQX, $n=35$; $N=12$). Mean values of peak currents are shown in the histograms. D) EB gel from nested RT-PCR amplification of insulin and AMPAR subunits. Each band is indicated by an arrow. Base-pairs were 214 (GRIA1), 369 (GRIA2), 172 (GRIA3), 201 (GRIA4) and 113 (insulin). Sequencing results of bands are listed in Table S1. E) The immunostaining of GluR2 in two islets. GluR2 and insulin were labeled with red and green, indicating that GluR2 was expressed in insulin-positive β cells. Scale bar: 40 μ m. **, $p < 0.01$.

response in 11 mM glucose (Figure 1B2) (15). After electrophysiological recordings, we performed single cell RT-PCR to detect the mRNA expressions of insulin and glucagon for further identification. Taking advantage of the giga-ohm seal that prevented contamination from the extracellular solution, we extracted the contents of individual cells into the recording pipette for the nested RT-PCR. As shown in Figure 1A3,B3, there was only an insulin band in β cells and only a glucagon band in α cells.

We then recorded glutamate receptor-mediated currents in identified β cells. At a holding voltage of -80 mV, local administration of $600 \mu\text{M}$ glutamate induced inward currents with a mean equilibrium amplitude of 81.3 ± 13.2 pA in β cells ($n=46$; $N=16$; Figure 1C). Likewise, local application of $100 \mu\text{M}$ (RS)- α -amino-3-hydroxy-5-methyl-4-isoxazolepropionic acid (AMPA) induced inward currents with a mean equilibrium amplitude of 89.2 ± 9.8 pA ($n=35$; $N=12$; Figure 1C). Addition of $10 \mu\text{M}$ CNQX or $40 \mu\text{M}$ GYKI53655, preferential antagonists of the AMPAR, significantly inhibited both glutamate and AMPA-induced currents, indicating the existence of functional AMPARs in β cells. We next used single cell RT-PCR to detect the mRNA expression of AMPA receptor subunits. Our results showed that transcripts of the AMPA receptor genes GRIA1 (GluR1), GRIA2 (GluR2), GRIA3 (GluR3) and GRIA4 (GluR4) were detected consistently in β cells that were identified by the only presence of insulin ($n=20$; Figure 1D). The sequencing results of the mRNAs were listed in Table S1. Specifically, we noticed that the amino acid at the Q/R site of GluR2 was arginine, which hinders Ca^{2+} entry through AMPARs (Table S1) (18). Furthermore, co-immunostaining of GluR2 and insulin were performed to confirm the expression of AMPARs in β cells (Figure 1E). Our results demonstrated that GluR2 was expressed in insulin positive cells in islets. Taken together, these results showed that Ca^{2+} -impermeable AMPARs are expressed in β cells, in agreement with previous results (9).

AMPARs participate in β -cell exocytosis and insulin release

We continued to explore whether AMPARs play roles in β cell exocytosis and insulin release. First, we examined the exocytosis induced by train-depolarization stimuli. Figure 2A shows the representative recordings obtained in control and glutamate groups. The mean incremental changes in C_m (ΔC_m) evoked by the individual pulses were present in Figure 2B ($n=19$; $N=5$). In control, ΔC_m increased from 5.9 ± 2.2 fF/pF (first pulse) to 30.2 ± 4.8 fF/pF (last pulse). In the glutamate group, ΔC_m increased from 15.0 ± 3.8 fF/pF (first pulse) to 64.0 ± 8.5 fF/pF (last pulse). The size of the readily releasable pool (RRP) ($\sum \Delta C_m_{1\text{st-2nd pulse}}$) (19–21) of vesicles was increased by 102% in glutamate groups (control: 11.4 ± 2.6 fF/pF versus glutamate: 23.1 ± 5.3 fF/pF). The membrane capacitance elicited by the entire train (total release) was increased by 113% in glutamate groups (control: 30.2 ± 4.8 fF/pF versus glutamate: 64.0 ± 8.5 fF/pF)

(Figure 2C). These data suggested that AMPAR activation increases the docking of insulin-containing granules.

Our previous work showed that, in 3 mM glucose, a 500 milliseconds depolarizing pulse leads to calcium influx and stimulates exocytosis (16). Thus, we assessed the depolarization-induced exocytosis and found that the mean capacitance increase was 60.2 ± 10.7 fF ($n=74$; $N=20$). We then tested the effect of AMPAR activation on β -cell exocytosis. After the first exocytosis measurement at 2 min, the cell was incubated with $600 \mu\text{M}$ glutamate for 2 min and exocytosis was measured again at 4 min (Figure 2D). We found that glutamate significantly increased the exocytosis (Figure 2E). In contrast, co-application of CNQX with glutamate significantly decreased the exocytosis at 6 min (Figure 2D,E). Decreased exocytosis in glutamate+CNQX might be due to the blockade of endogenous glutamate action because glutamate exists in the extracellular space of islets (9). For this reason, we applied CNQX alone and found that the exocytosis decreased to $55.6 \pm 9.3\%$ of control ($n=11$; $N=3$; Figure S1). These data suggested that AMPAR activation participates in the exocytosis.

To determine the effects of AMPARs on insulin secretion, we performed ELISA tests in mouse islets. We found that, in 5 mM glucose, neither glutamate nor glutamate+CNQX affected the insulin secretion ($n=3$ experiments; Figure 2F). In 16.7 mM glucose, glutamate raised the insulin release while glutamate+CNQX reduced it ($n=3$ experiments; Figure 2F). These data demonstrated that the activation of AMPARs increases insulin secretion in the high glucose.

Glutamate increases docking of insulin-containing granules

Docked insulin-containing granules are responsible for insulin release (22,23). So, we went on to determine whether the number of docked insulin-containing granules changed after glutamate challenge using time-lapse TIRFM. After transfection with insulin-eGFP (24), β cells were consecutively treated with control saline, glutamate and glutamate+CNQX at 30°C . TIRFM imaging started 2 min after each chemical treatment (Movie S1–S3). Representative images are shown in Figure 3A. Fluorescent particles were counted as insulin-containing granules only if their fluorescence intensities were threefold higher than the background level and their diameters were ≥ 200 nm and ≤ 666 nm (Figure 3B,C) (24). We calculated the 3D displacement [$R^{(3)}$] of each vesicle to identify docked granules (Figure S2). Our results showed that the numbers of docked granules were 15.4 ± 2.6 (control), 27.6 ± 3.3 (glutamate) and 13.0 ± 3.9 (glutamate+CNQX) ($n=5$; $N=4$; Figure 3D). These data demonstrated that glutamate increases the number of docked insulin-containing granules. We also noticed that there was no vesicle that suddenly brightened and vanished within 300 milliseconds [fusion event (22)] either in the basal state or after the glutamate application at both 5 Hz ($n=5$; Figure S2B)

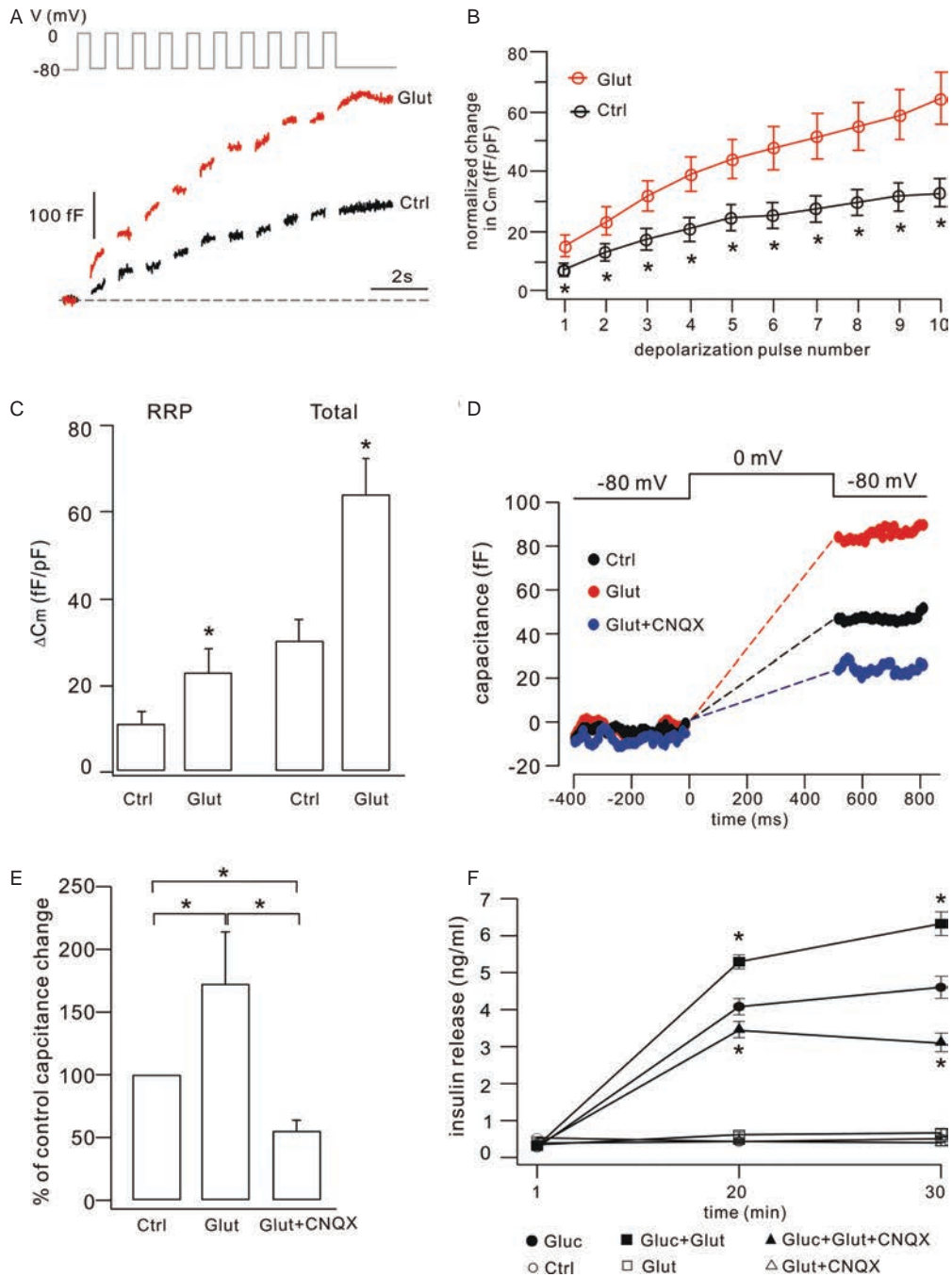


Figure 2: AMPARs modulate exocytosis and insulin release. A) Representative recordings of capacitance changes (ΔC_m) from β cells that were stimulated by a train depolarization stimuli shown in the above (-80 to 0 mV; 500 milliseconds; 1 Hz). Responses of control and glutamate groups are indicated as black (Ctrl) and red (Glut). B) The mean incremental changes in C_m (ΔC_m) evoked by the individual pulses (Ctrl: $n = 18$; $N = 5$; Glut: $n = 20$; $N = 5$). C) Statistics of RRP ($\sum \Delta C_m_{1st-2ndpulse}$) and total release in control (Ctrl; $n = 18$; $N = 5$) and glutamate (Glut; $n = 20$; $N = 5$) groups. D) Single depolarization-evoked exocytotic responses derived from one β cell in control, glutamate, and co-application of glutamate and CNQX. This cell was voltage-clamped at -80 mV and then depolarized to 0 mV for 500 milliseconds to induce exocytosis. The responses were obtained at 2 (black), 4 (red) and 6 (blue) min. Capacitance changes were defined as the difference between capacitances before and after depolarization. Responses during depolarization were omitted (dashed lines) because of irregular spikes (19). E) Capacitance changes from experiments as in D were 83.5 ± 12.9 fF (Glut, $n = 60$; $N = 20$) and 33.4 ± 9.4 fF (Glut+CNQX, $n = 47$; $N = 20$). F) Insulin release in either 16.7 mM (filled symbols) or 5 mM (unfilled symbols) glucose. At 16.7 mM glucose, glutamate ($600 \mu M$) raised the insulin release to 5.3 ± 0.2 ng/mL (20 min) and 6.3 ± 0.3 ng/mL (30 min), compared to control (20 min: 4.1 ± 0.2 ng/mL; 30 min: 4.6 ± 0.3 ng/mL). Glutamate+CNQX reduced the insulin release to 3.5 ± 0.2 ng/mL (20 min) and 3.1 ± 0.3 ng/mL (30 min). *, $p < 0.05$.

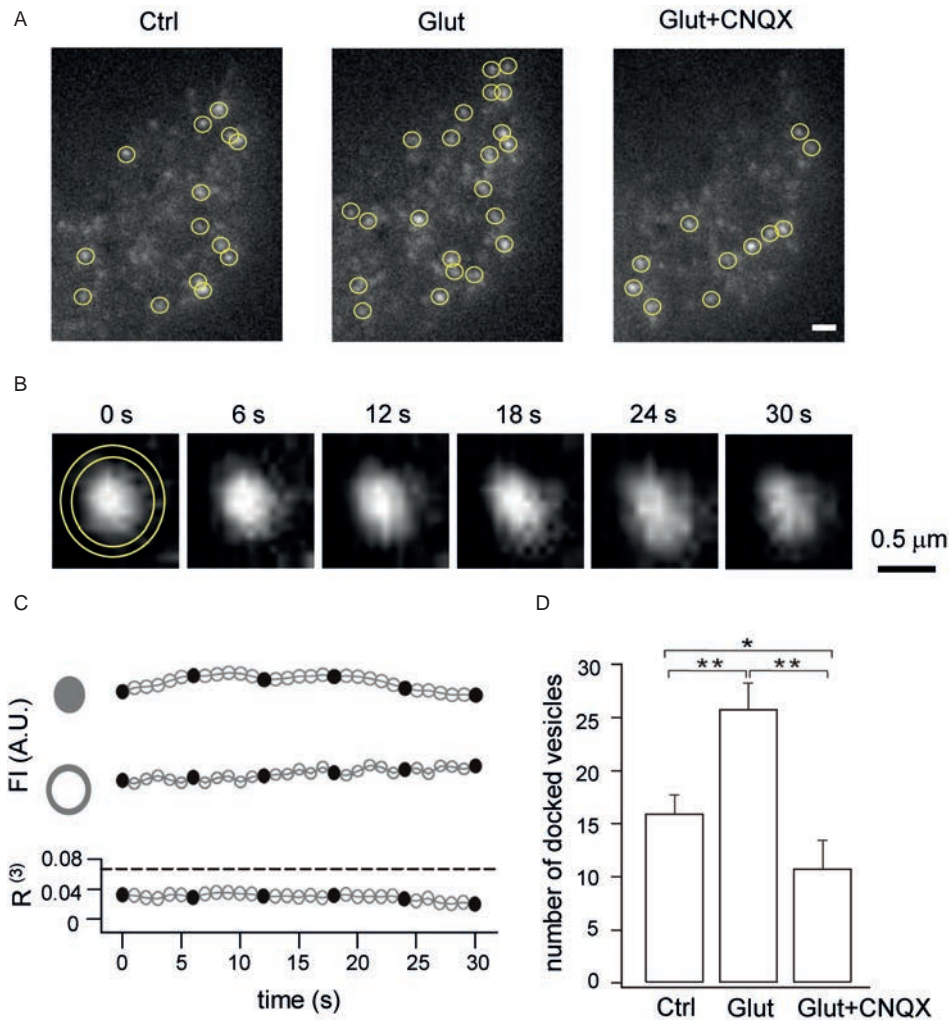


Figure 3: Glutamate increases docking of insulin-containing granules. A) TIRFM images of GFP-labeled insulin granules in one β cell in Ctrl, Glut and Glut+CNQX. Yellow circles indicate insulin-containing granules. Scale bar, 2 μm . See Movies S1–S3 for series of images. B) A typical sequential images of a docked vesicle. Times indicated above are relative to the beginning of the imaging period. To analyze the fluorescence, the inner circle and the annulus are depicted with a diameter of 0.75 and 0.9 μm centered on the vesicle. C) Time courses of the fluorescence intensity (FI) in arbitrary units (AU) from the inner and annular areas and $R^{(3)}$ of the vesicle shown in (B). Horizontal dashed line marks the level of 0.067 μm , which was used as the threshold to identify docking. Filled circles indicate the time points of the images in (B). D) Numbers of docked events are plotted in control (Ctrl), glutamate (Glut) and glutamate with CNQX (Glut+CNQX). *, $p < 0.05$; **, $p < 0.01$.

and 20 Hz ($n=5$) of TIRFM scanning (data not shown), consistent with previous work (22), implying that glutamate does not induce fusion event.

Glutamate increases cytosolic Ca^{2+}

It is well known that the exocytosis of insulin-containing granules is $[\text{Ca}^{2+}]_i$ -dependent (25,26). To investigate whether glutamate application increased $[\text{Ca}^{2+}]_i$, we observed confocal images of Ca^{2+} fluorescence in β cells after filling them with 80 μM Fluo-4 in the ATP-free recording pipette solution. Glutamate induced an increase in fluorescence intensity (Figure 4A,B). When the external $[\text{Ca}^{2+}]$ was switched to 0, glutamate application did not change $[\text{Ca}^{2+}]_i$ (Figure 4A,B). These results demonstrated

that the glutamate-induced increase of $[\text{Ca}^{2+}]_i$ depends on extracellular Ca^{2+} influx, which is intriguing because AMPARs in β cells are impermeable to Ca^{2+} due to the existence of GluR2 subunits (Figure 1D,E; Table S1) (18). It is known that K_{ATP} channels control the gating of VGCCs and Ca^{2+} influx (27). In order to test whether the glutamate-evoked Ca^{2+} transient was related to K_{ATP} channels, Ca^{2+} imaging was re-examined when 10 mM internal ATP (17,28,29) or 100 μM tolbutamide, a selective K_{ATP} channel blocker, was added to inhibit K_{ATP} channels. We noticed that the basal $[\text{Ca}^{2+}]_i$ was elevated and glutamate failed to induce further increase in both conditions (Figure 4A,B). We also observed Ca^{2+} transient with the application of 10 μM nifedipine, a VGCC blocker.

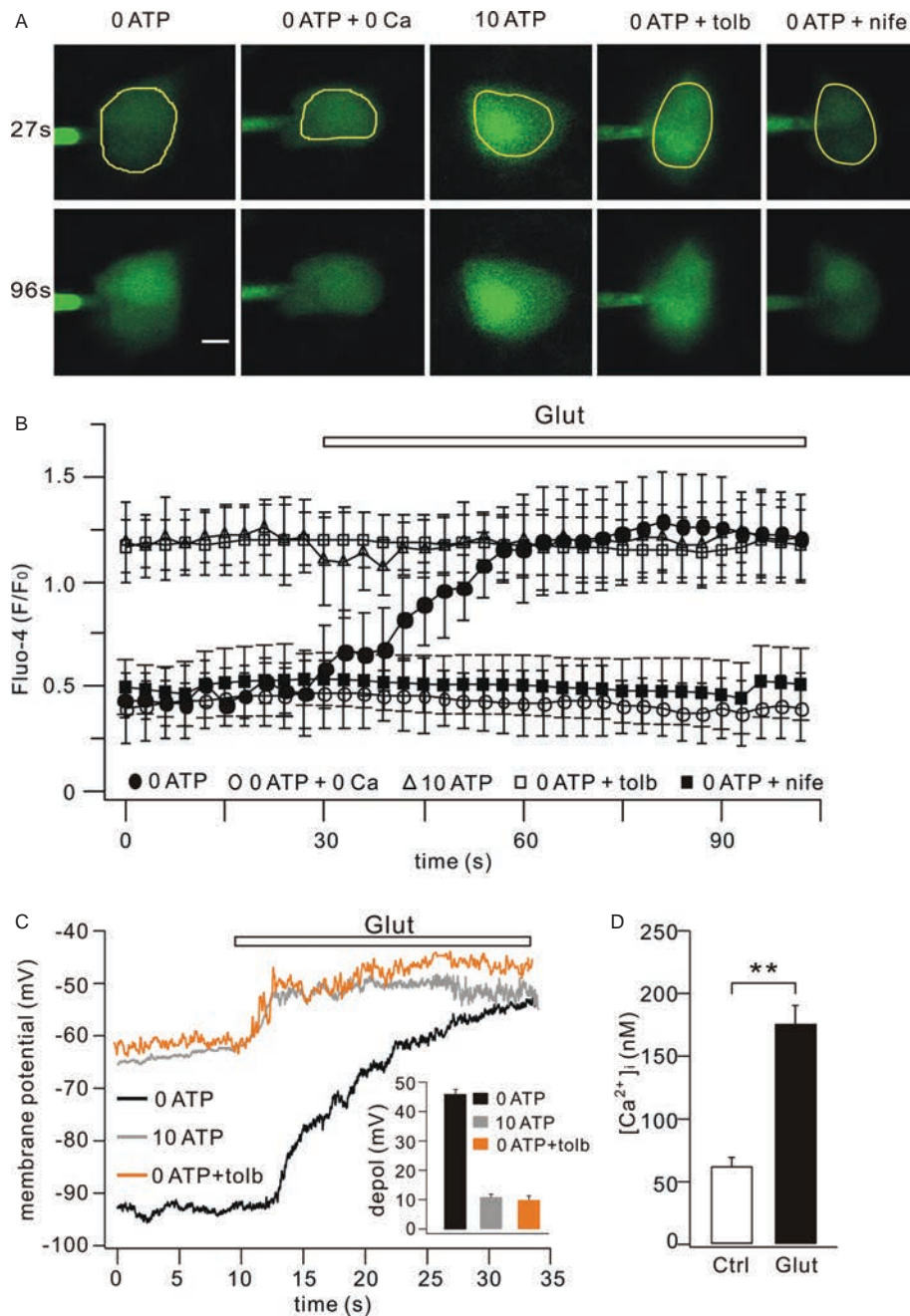


Figure 4: AMPAR activation increases cytosolic Ca^{2+} . A) $[Ca^{2+}]_i$ responses were monitored every 1 second and glutamate (600 μ M) was introduced after 30 seconds of baseline observation. The same microscopic fields are shown before (27 seconds) and after (96 seconds) glutamate stimulation. '0 ATP', '0 ATP+0 Ca', '10 ATP', '0 ATP+tolb' and '0 ATP + nife' represent $[Ca^{2+}]_i$ responses in 0 mM internal ATP, 0 mM internal ATP with 0 external calcium, 10 mM internal ATP, 0 mM internal ATP with 100 μ M tolbutamide and 0 mM internal ATP with 10 μ M nifedipine. Yellow outlines indicate the regions of interest where foreground Fluo-4 fluorescence was measured. Scale bar, 2.5 μ m. B) Time-course of Fluo-4 fluorescence (F/F_0) in different conditions. Six hundred micromolar of glutamate (top bar) induced an increase in fluorescence intensity that reached a plateau (F/F_0 : 1.25 ± 0.01 ; $n=10$, $N=5$) relative to the baseline (F/F_0 : 0.45 ± 0.01 ; $n=10$, $N=5$). Glutamate did not change $[Ca^{2+}]_i$ without external Ca^{2+} ($n=7$; $N=4$) or in the presence of nifedipine ($n=16$; $N=7$). The resting $[Ca^{2+}]_i$ level was elevated in 10 mM internal ATP ($n=5$; $N=2$) and 0 internal ATP with 100 μ M tolbutamide ($n=14$; $N=3$). Glutamate failed to change $[Ca^{2+}]_i$ in these two conditions. C) Membrane potential in 0 (black), 10 mM (gray) internal ATP and 0 ATP+100 μ M tolbutamide (orange). The insert shows the increases of membrane potential by glutamate stimuli in 0 ATP ($n=8$; $N=3$), 10 mM internal ATP (10 ATP; $n=8$; $N=3$) and 0 ATP with 100 μ M tolbutamide (0 ATP+tolb; $n=9$; $N=3$). The membrane potential increase was 46.2 ± 1.7 mV (0 ATP), 10.9 ± 1.0 mV (10 ATP) and 10.2 ± 1.2 mV (0 ATP+tolb). D) $[Ca^{2+}]_i$ in control (Ctrl, 60 ± 15 nM, $n=20$; $N=5$) and glutamate (Glut, 176 ± 13 nM, $n=9$; $N=3$). *, $p < 0.05$. **, $p < 0.01$.

Our results revealed that Ca^{2+} influx was blocked by nifedipine (Figure 4A). These data indicated that AMPARs increase a depolarization to enhance $[\text{Ca}^{2+}]_i$.

In order to examine the depolarization induced by glutamate application, we recorded the membrane potential using current-clamp configuration. The averaged resting membrane potential of β cells was -95 ± 1 mV when the pipette solution was filled with 0 mM ATP (Figure 4C). Glutamate application (20 seconds) induced a significant membrane depolarization to -49 ± 2 mV (Figure 4C). We next measured the glutamate-induced direct depolarization in β cells by applying 10 mM internal ATP or 100 μM tolbutamide to inhibit K_{ATP} channels. β cells were depolarized in the presence of 10 mM internal ATP (resting potential: -65 ± 1 mV) or 100 μM tolbutamide (-60 ± 1 mV), compared to the condition of 0 internal ATP. Application of glutamate (20 seconds) was able to further depolarize β cells to -54 ± 1 mV (10 ATP) and -49 ± 1 mV (100 μM tolbutamide). These data indicated that AMPAR activation can induce a direct depolarization. Also, AMPAR activation is able to induce a much bigger depolarization when K_{ATP} channels are available.

Previous work reported that 500 nM $[\text{Ca}^{2+}]_i$ causes the exocytosis of insulin-containing granules (30,31), while lower concentrations (100–500 nM) rather promote the docking of insulin-containing granules (32). In order to determine whether glutamate-induced depolarization and Ca^{2+} influx was strong enough to evoke insulin release, we used Fura-PE3 ratiometric imaging to assess to what extent glutamate elicited a rise in $[\text{Ca}^{2+}]_i$ (30,33). In the absence of glutamate, the $[\text{Ca}^{2+}]_i$ was low (60 ± 15 nM; $n=9$; $N=3$; Figure 4D). External glutamate (600 μM) led to an about threefold increase of $[\text{Ca}^{2+}]_i$ (176 ± 13 nM; $n=8$; $N=3$; $p < 0.01$), which was similar to the Fluo-4 imaging results (Figure 4B). This limited $[\text{Ca}^{2+}]_i$ increase tends to trigger the docking of insulin granules rather than direct exocytosis, as illustrated in Figure 3.

Effects of AMPARs are deficient in Kir6.2 knock-out mice

We repeated exocytosis and insulin measurements as well as confocal Ca^{2+} imaging in Kir6.2 knock-out mice, in which the functions of K_{ATP} channels are absent (34). Distinct from wild-type cells, we found that neither glutamate nor glutamate+CNQX affected the capacitance in knock-out cells (Figure 5A). We next measured insulin in islets isolated from knock-out mice by ELISA and found that neither glutamate nor glutamate+CNQX significantly changed the insulin secretion in both 5 and 16.7 mM glucose (Figure 5B). Finally, we found that 600 μM glutamate failed to induce any change in Fluo-4 fluorescence (Figure 5C).

Glutamate signaling modulates K_{ATP} channel conductance and voltage oscillation

To investigate how K_{ATP} channels were modulated by AMPARs, K_{ATP} channel conductance was measured using

whole-cell patch-clamp in a K^+ -based ATP-free pipette solution (28,33,35). After establishing the whole-cell configuration, K_{ATP} conductance rapidly increased to a peak, usually within 2 min, with a mean maximum of 3.9 ± 0.1 nS/pF ($n=20$; $N=6$; Figure 6A). Glutamate treatment reduced the peak amplitude to 3.1 ± 0.2 nS/pF ($n=20$; $N=6$; $p < 0.05$). Co-application of glutamate with CNQX reversed this phenomenon (4.6 ± 0.2 nS/pF; $n=20$; $N=6$). We also compared the effects of glutamate on K_{ATP} conductance when increasing the pipette ATP concentration. With 3 mM internal ATP, glutamate application reduced the peak amplitude (Figure 6B). As well as the conductance, we further recorded K_{ATP} currents evoked by hyperpolarizing and depolarizing pulses from a holding potential of -80 mV. K_{ATP} currents were completely blocked by 100 μM tolbutamide (Figure 7A). Glutamate was pre-treated 2 min before and continuously applied during the step-command stimuli (Figure 7A). We found that glutamate decreased but glutamate+CNQX increased the K_{ATP} currents (Figure 7A1,B). Given these data, we concluded that glutamate signaling modulates the conductance of K_{ATP} channels. To exclude the potential effects from neighboring cells, β cells were continuously perfused with mefloquine, a gap junction inhibitor, and K_{ATP} channel conductance was recorded. Application of glutamate significantly decreased the maximal conductance of K_{ATP} channels (Figure S3), suggesting that the effects of AMPARs on K_{ATP} channels are not mediated by neighboring cells.

Closure of K_{ATP} by cytosolic ATP induces a typical spontaneous burst-like membrane voltage oscillation (17), which is a determining factor for insulin secretion in the β cells (17,29). Therefore, we investigated the effects of AMPARs on the K_{ATP} -dependent voltage oscillations (17). After baseline recording for 8–10 min, glutamate and glutamate+CNQX were sequentially perfused to assess their effects on the oscillations (Figure 8A). The average amplitude and duration of spikes were 12.7 ± 0.9 mV and 8.3 ± 0.5 seconds in controls (Figure 8B; 40 spikes; $n=10$; $N=4$), similar to previous findings (16). Glutamate increased, while glutamate+CNQX significantly attenuated burst amplitude and burst duration (Figure 8C). These data further confirmed that AMPARs modulate K_{ATP} channels.

Effects of AMPARs on K_{ATP} channels are cGMP-dependent

Previous work demonstrated that K_{ATP} channels are regulated by cyclic GMP (cGMP) (36,37). In cerebellar cells, AMPAR activation increases cGMP levels (38,39). Thus, we hypothesized that AMPAR activation might increase cGMP and subsequently inhibit K_{ATP} channels. To test this hypothesis, K_{ATP} conductance was measured by application of internal 100 μM cGMP and external 20 μM ODO (1H-[1,2,4]oxadiazolo[4,3-a]quinoxalin-1-one), an inhibitor of cGMP synthesis (40). With cGMP in the pipette solution, the average amplitude of K_{ATP} conductance was significantly reduced compared to control (Figure 9A,B).

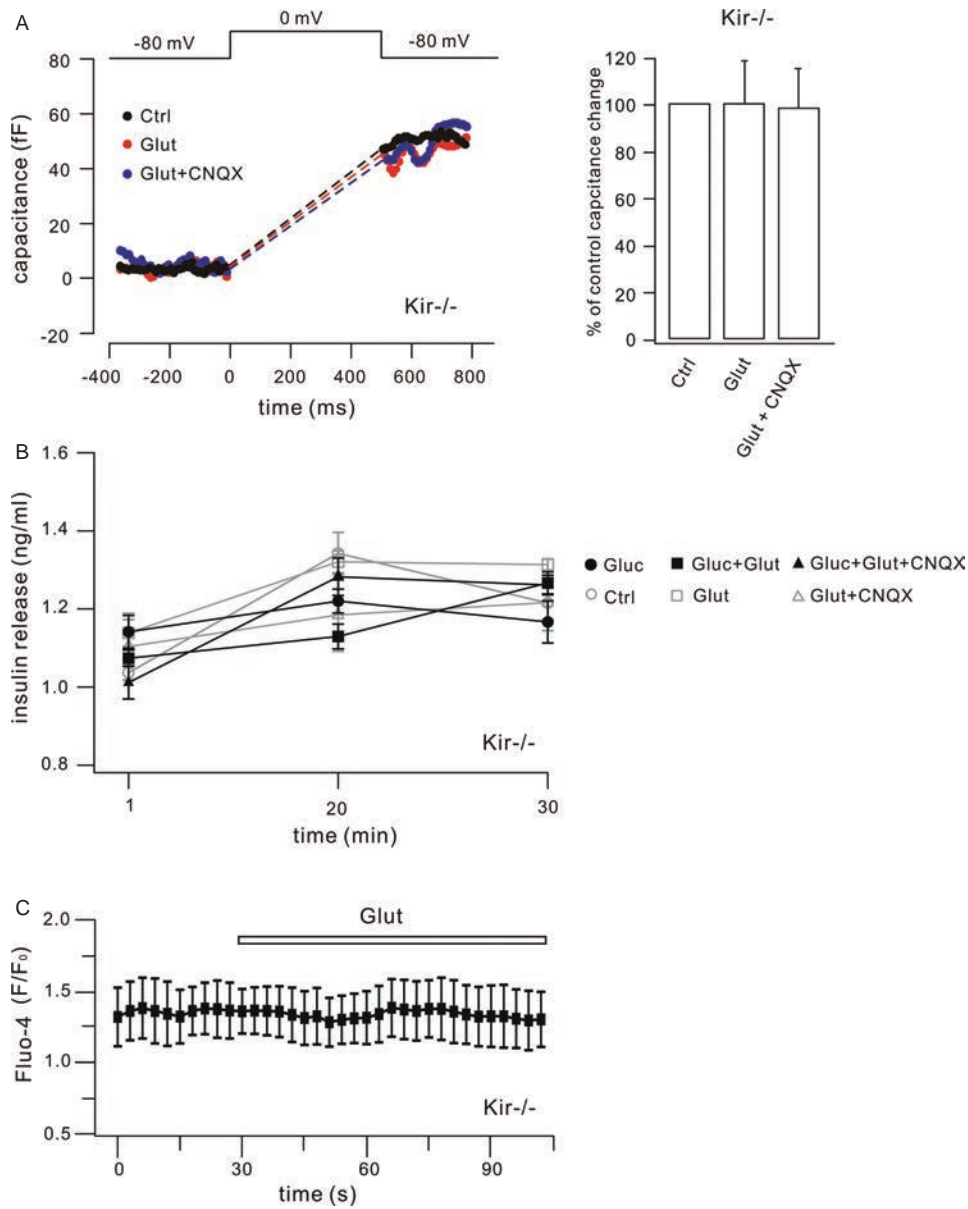


Figure 5: Effects of AMPARs are deficient in Kir6.2 knock-out mice. A) Depolarization-induced exocytotic responses from a Kir6.2^{-/-} β cell. After 2-min recording, the cell was depolarized to 0 mV for 500 milliseconds to induce membrane exocytosis. Exocytosis tests were repeated at 2 (black), 4 (Glut, red) and 6 (Glut+CNQX, blue) min. Glutamate application did not change the capacitance ($100 \pm 18\%$ of control; $n = 18$; $N = 8$), and neither did glutamate+CNQX ($99 \pm 16\%$ of control; $n = 14$; $N = 6$) (bar graph in right). B) Insulin release in either 16.7 mM (filled symbols) or 5 mM (unfilled symbols) glucose ($n = 3$ experiments). With 16.7 mM glucose, released insulin at 30 min was 1.2 ± 0.07 (Ctrl), 1.3 ± 0.01 (Glut), 1.2 ± 0.04 (Glut+CNQX), 1.2 ± 0.05 (Gluc), 1.3 ± 0.02 (Gluc+Glut) and 1.3 ± 0.03 ng/mL (Gluc+Glut+CNQX). C) Time-course of Fluo-4 imaging in Kir^{-/-} β cells is shown. Kir^{-/-} cells were loaded with $80 \mu\text{M}$ Fluo-4 and 0 internal ATP and $[\text{Ca}^{2+}]_i$; responses were monitored every 1 second ($n = 12$; $N = 6$). Glutamate application is indicated by the top bar.

Glutamate failed to further decrease the conductance in the presence of cGMP (Figure 9A,B), implying that excessive cGMP prevents the action of glutamate. When the cGMP production was inhibited by ODQ, glutamate stimulation did not reduce K_{ATP} conductance compared to control (Figure 9A,B). This inhibition by ODQ was reversed by adding internal cGMP (Figure 9A,B).

Finally, we measured the cGMP concentration in β cells and found that glutamate significantly increased the concentration, while $5 \mu\text{M}$ *t*ACPD, the mGluR agonist, failed to induce any change (Figure 9C). cGMP concentrations were 9.8 ± 0.3 nM (Ctrl, $n = 20$; $N = 6$), 10.8 ± 0.2 nM (Glut, $n = 10$; $N = 4$) and 9.6 ± 0.5 nM (*t*ACPD, $n = 10$; $N = 4$). These data clearly indicated that the activation of AMPARs

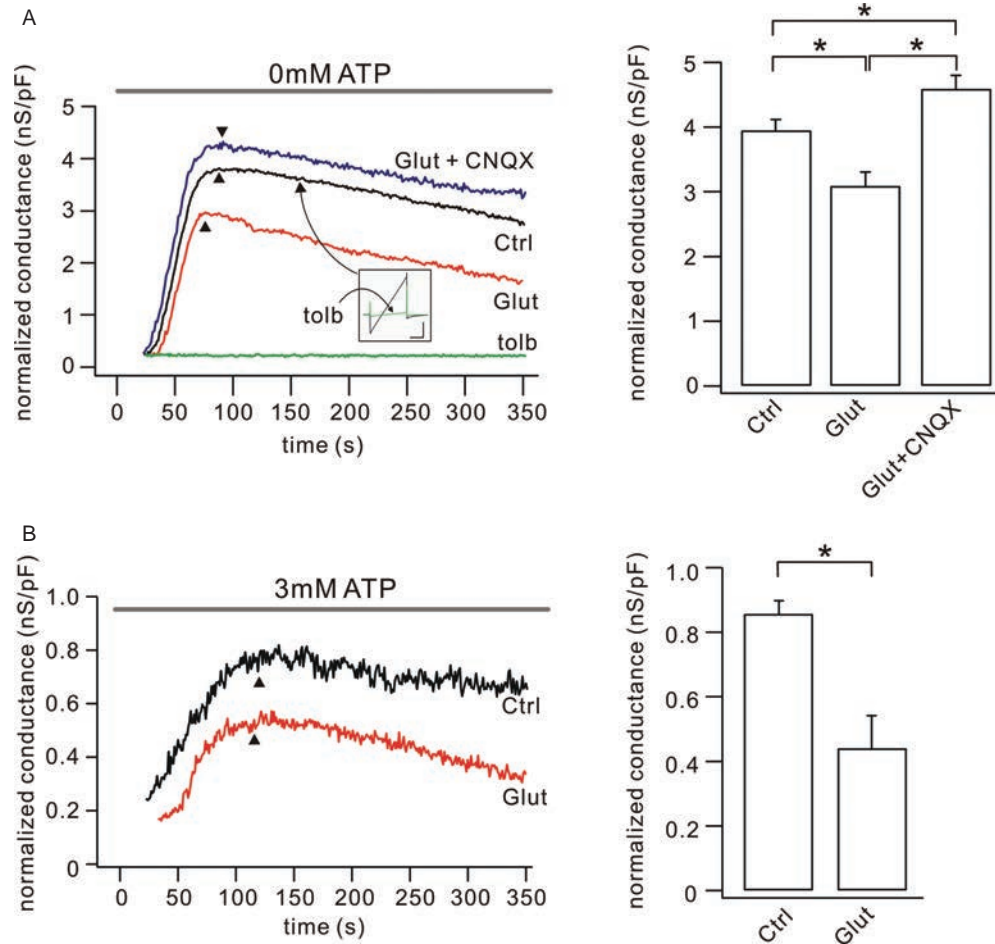


Figure 6: AMPAR activation attenuates K_{ATP} channel conductance. A) K_{ATP} conductance measured by internal dialysis with 0 ATP in the pipette. Black, red and blue traces show K_{ATP} conductance in ECS (Ctrl), glutamate (Glut) and glutamate with CNQX (Glut+CNQX). Black triangles show the peak of each response. The short duration between rupture (0 second) and the first data point was used for membrane capacitance compensation. Note that differences in the times to maximum were probably due to different cell sizes and pipette tips, which affected the diffusion rate (35). Each conductance data point was acquired from one ramp (100 milliseconds) stimulation that was given at 1 Hz. The insert shows representative ramp currents in control (black) and tolbutamide (green). Tolbutamide inhibited the ramp-stimulated current, indicating that the current was K_{ATP} channel-mediated. Scale bars in inset, 30 milliseconds, 200 pA. The green trace labeled 'tolb' shows the K_{ATP} conductance with tolbutamide. Right panel shows the statistics of maximal K_{ATP} conductance in different conditions. B) Typical conductances measured from two cells internally dialyzed with 3 mM ATP in the pipette. Traces show K_{ATP} conductance in control (Ctrl, black) and glutamate (Glut, red). Black triangles show the peak of each response. Maximal K_{ATP} conductance were 0.86 ± 0.04 (Ctrl; $n = 11$; $N = 4$) and 0.44 ± 0.10 (Glut; $n = 11$; $N = 4$) (right panel). *, $p < 0.05$.

increases the cGMP production in β cells, which in turn decreases the conductance of K_{ATP} channels (36,37).

Discussion

Using whole-cell patch-clamp recording combined with nested RT-PCR and immunohistochemistry, we showed that functional GluR2-containing AMPARs are expressed in mouse β cells. Our results further showed that the activation of AMPARs affects the conductance of K_{ATP} channels and their-mediated membrane voltage oscillation, increases the $[Ca^{2+}]_i$ and docking of insulin-containing granules to the plasma membrane,

and therefore modulates insulin release. Finally, we demonstrated that the effects of AMPARs on K_{ATP} channels require cGMP production. Interestingly, CNQX alone also significantly reduced exocytosis (Figure S1). Therefore, we concluded that endogenous glutamate participates in exocytosis in β cells.

It is controversial whether functional iGluRs are expressed in β cells (4–6,11). Cabrera et al. (11) found no iGluRs in mouse β cells by showing that the iGluR agonist, kainite, fails to trigger insulin release under low glucose levels, which was also found in our insulin detection in the similar glucose concentration (Figure 1F). These results may be due to the low glucose concentration,

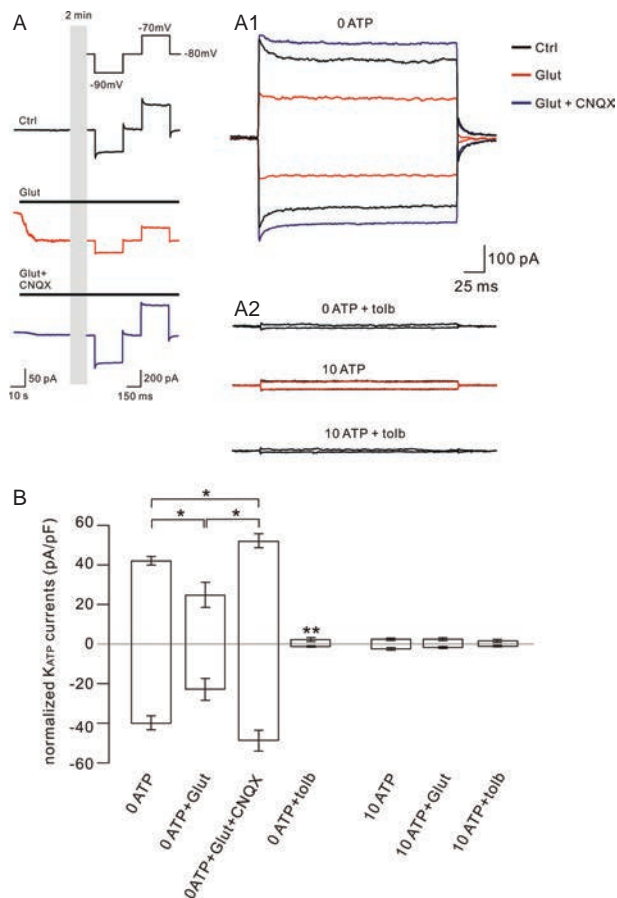


Figure 7: K_{ATP} channel-mediated currents. A) Representative K_{ATP} currents derived from β cells with 0 ATP in the pipette. Cells were voltage-clamped at -80 mV and pre-treated with control (Ctrl, black), glutamate (Glut, red) or glutamate+CNQX (Glut+CNQX, blue) for 2 min as indicated by black bars. The gray bar shows the cell stabilization time before step voltage stimuli. Afterward, cells were sequentially hyperpolarized to -90 mV and depolarized to -70 mV each for 300 milliseconds. A1) Step voltage-induced currents derived from (A) are superimposed. A2) External tolbutamide (0 ATP+tolb; 10ATP+tolb) and 10 mM internal ATP (10 ATP; 10ATP+tolb) effectively inhibited step voltage-induced currents, indicating they were mediated by K_{ATP} channels. Scale bars for (A1) and (A2) are shown in right. B) Amplitudes of K_{ATP} currents in different conditions calculated as current density (current amplitude/cell capacitance). The upward and downward bars indicate the depolarizing and hyperpolarizing currents. For depolarization, averaged current densities were 42.5 ± 2.1 pA/pF (0 ATP; $n=6$, $N=3$), 25.2 ± 6.3 pA/pF (0 ATP+Glut; $n=6$, $N=3$), 53.0 ± 3.4 pA/pF (0 ATP+Glut+CNQX; $n=6$, $N=3$), 2.5 ± 0.3 pA/pF (0 ATP+tolb; $n=6$, $N=3$), 3.9 ± 0.2 pA/pF (10 ATP; $n=6$, $N=3$), 3.1 ± 0.2 pA/pF (10 ATP+Glut; $n=6$, $N=3$), 1.7 ± 0.3 pA/pF (10 ATP+tolb; $n=6$, $N=3$). For hyperpolarization, averaged current densities were -40.6 ± 3.5 pA/pF (0 ATP; $n=6$, $N=3$), -22.6 ± 5.2 pA/pF (0 ATP+Glut; $n=6$, $N=3$), -47.6 ± 5.3 pA/pF (0 ATP+Glut+CNQX; $n=6$, $N=3$), -1.2 ± 0.3 pA/pF (0 ATP+tolb; $n=6$, $N=3$), -2.7 ± 0.3 pA/pF (10 ATP; $n=6$, $N=3$), -2.5 ± 0.4 pA/pF (10 ATP+Glut; $n=6$, $N=3$), -1.3 ± 0.4 pA/pF (10 ATP+tolb; $n=6$, $N=3$). *, $p < 0.05$. **, $p < 0.01$.

because we found that glutamate application increased the insulin release in the high glucose condition (Figure 2F). Besides, our other experiments proved that functional AMPARs are expressed in mouse β cells: (i) single cell RT-PCR experiments detected that mRNAs of AMPARs were expressed in identified β cells (Figure 1D); (ii) immunostaining experiments clearly indicated that GluR2 was expressed in insulin-positive β cells (Figure 1E); (iii) glutamate application enhanced β cell exocytosis (Figure 2) and (iv) AMPAR activation significantly increased the influx of extracellular Ca^{2+} (Figure 4). Furthermore, we found that AMPAR activation increased $[Ca^{2+}]_i$ (Figure 4) and assisted more insulin-containing granules docking onto the plasma membrane (Figure 3), which consists of RRP (26). Our $[Ca^{2+}]_i$ measurement showed that the $[Ca^{2+}]_i$ elevation elicited by glutamate stimulation was rather limited (Figure 4D), which helped to increase the docking, but was far from the requirement for the insulin release (>500 – 800 nM) (30–32). The increase of RRP by glutamate application was also proved in the exocytosis evoked by train depolarization (Figure 2C). These results explain why glutamate increased insulin release only in the high glucose level (Figure 2F). Glutamate application increased the docked granules, which were not released by the weak driving force, for example, the low-glucose used in previous (11) and the current work (Figure 2F), but were released by the strong driving force, for example, depolarization or high glucose (Figure 2).

One important finding in the current work was that AMPAR activation increased cytosolic cGMP to inhibit K_{ATP} channels. K_{ATP} channels are essential for modulating the internal $[Ca^{2+}]_i$ (27). Closure of K_{ATP} causes Ca^{2+} influx and subsequent exocytosis (26,41,42). Thus, AMPAR activation caused the inhibition of K_{ATP} channels and increased the internal free Ca^{2+} and the number of docked granules. The K_{ATP} channel-dependence of AMPARs' effects on insulin release was enforced by our evidence that: (i) activation of AMPARs reduced the conductance and whole-cell current of K_{ATP} channels (Figure 6 and 7); (ii) supplementing with cytosolic cGMP inhibited the conductance of K_{ATP} channels and glutamate significantly increased the concentration of cGMP in β cells. AMPAR effects disappeared if cGMP production was blocked by ODQ (Figure 9); (iii) glutamate application increased the K_{ATP} channel-mediated voltage oscillation (Figure 8).

We showed that glutamate application induced direct depolarization as well as another much bigger depolarization when K_{ATP} channels were available (Figure 4C). While both assist to depolarize β cells, it might be deduced that the bigger depolarization plays more important roles in β cell exocytosis. The resting membrane potential of β cells is around -80 mV in normal cytosolic ATP condition [~ 3 mM (28)], in which K_{ATP} channels are active (17,28). Similarly, we showed that, in 0 ATP, glutamate significantly depolarized β cells from -95 to -50 mV (Figure 4C) through closing K_{ATP} channels (Figure 6). The relationship between AMPARs and K_{ATP} channels was supported

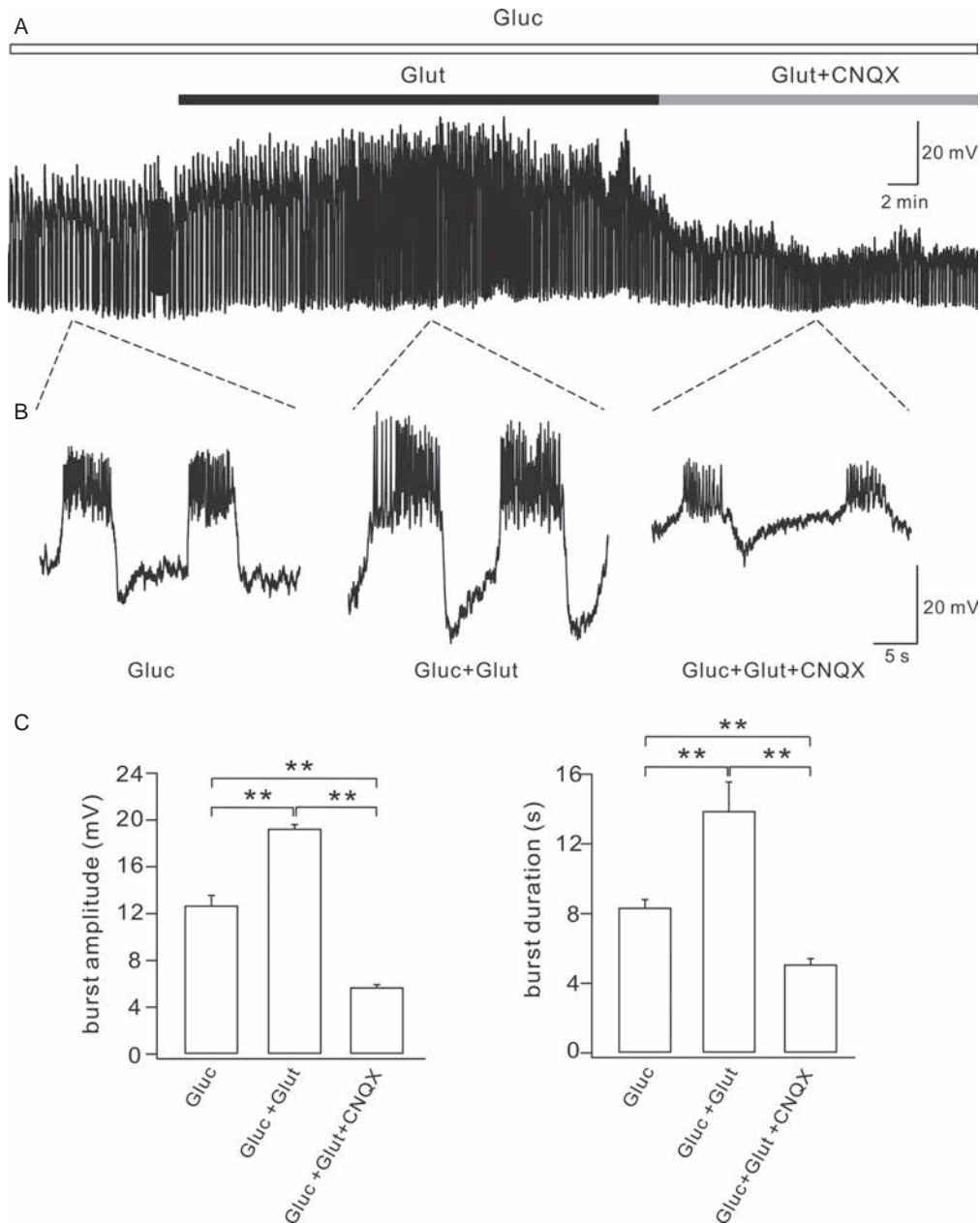


Figure 8: AMPAR activation modulates burst oscillations. β cells were perfused with a background solution containing 11 mM glucose, which elicited stable bursts that usually appeared within 30 min after break-in and reliably lasted as long as the whole-cell recording continued. A) Example of β cell burst oscillation. Glucose (Gluc; 11 mM) was introduced to evoke burst oscillation in this β cell. After 10-min baseline recording, 600 μ M glutamate (Glut) and 600 μ M glutamate+10 μ M CNQX were consecutively added, as indicated by black and gray bars. The basal membrane potential slightly increased with 9.8 ± 1.7 mV ($n=6$, $N=3$) upon the application of glutamate. B) Representative adjacent pairs of spikes randomly selected from Gluc, Gluc+Glut and Gluc+Glut+CNQX conditions, as indicated by dashed lines. To quantify the bursts evoked by glucose, the duration and amplitude of bursts were measured under different drug applications. C) Statistics of burst amplitude and duration on bath application of glucose (Gluc), glucose with glutamate (Gluc+Glut) and glucose with glutamate and CNQX (Gluc+Glut+CNQX). **, $p < 0.01$.

by our experiments that glutamate application produced cGMP and decreased the conductance of K_{ATP} channels (Figures 6, 7 and 9). These data suggested that AMPAR- K_{ATP} channel pathway-mediated depolarization may enormously depolarize β cells from a much hyperpolarized

status in normal cytosolic ATP levels and lead to increase of $[Ca^{2+}]_i$ and number of docked granules (Figure 3).

In conclusion, our results revealed a novel role of AMPARs in β cells, which is summarized by a model in Figure 10.

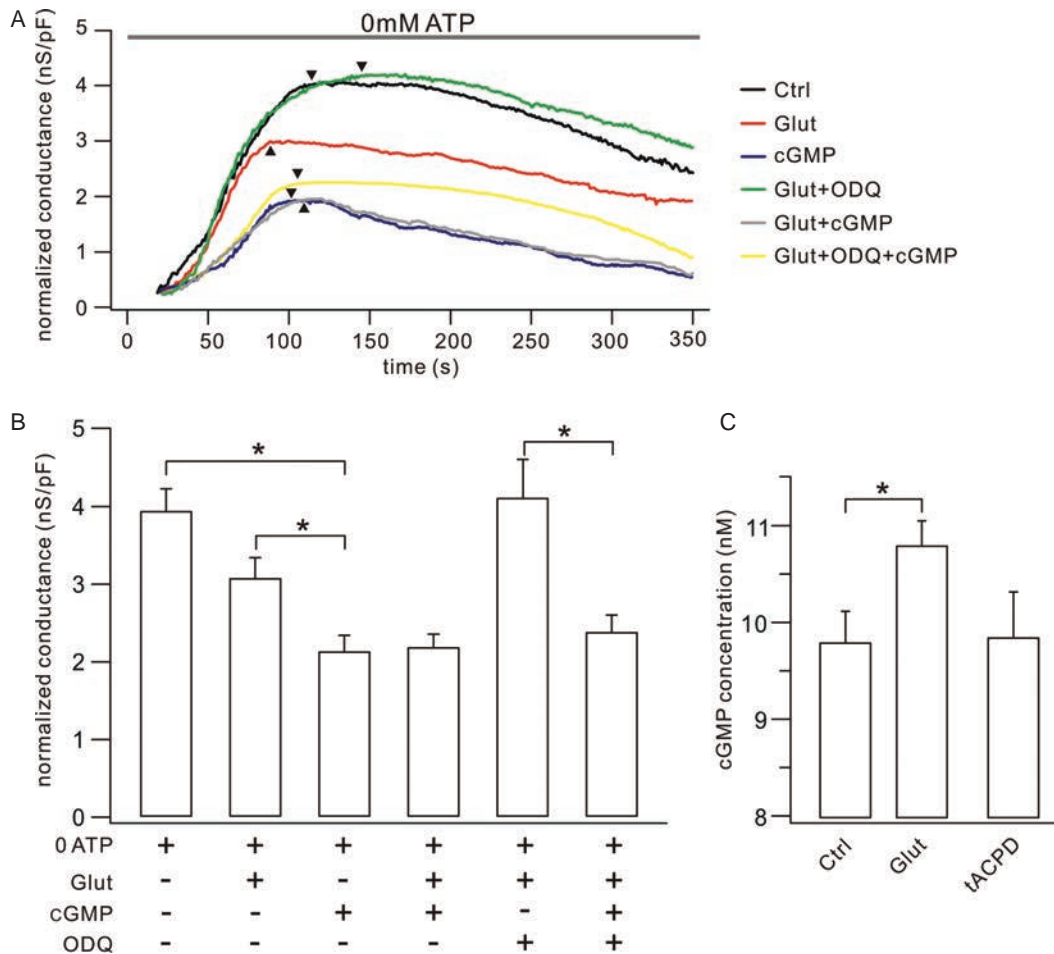


Figure 9: Effects of AMPAR require cGMP. A) K_{ATP} conductance measured by internal dialysis with 0 ATP in the pipette. Traces represent K_{ATP} conductance recorded in control (Ctrl, black), glutamate (Glut, red), cGMP (cGMP, blue), glutamate with cGMP (Glut+cGMP, gray), glutamate with ODQ (Glut+ODQ, green) and glutamate with ODQ and cGMP (Glut+ODQ+cGMP, yellow). Black triangles show the peak of each response. Short durations between rupture (0 second) and the first data point were used for membrane capacitance compensation. Note that differences in the times to maximum were probably due to different cell sizes and pipette tips. Each conductance data point was acquired from one ramp (100 milliseconds) stimulation that was given at 1 Hz. The Y-axis is the normalized value of conductance divided by cell capacitance. B) Statistics of normalized conductance. The mean values of conductance were 3.9 ± 0.1 nS/pF (Ctrl, $n = 20$; $N = 6$), 3.1 ± 0.2 nS/pF (Glut, $n = 20$; $N = 6$), 2.1 ± 0.2 nS/pF (cGMP, $n = 15$; $N = 6$), 2.2 ± 0.2 nS/pF (Glut+cGMP, $n = 10$; $N = 4$), 4.1 ± 0.5 nS/pF (Glut+ODQ, $n = 7$; $N = 2$) and 2.4 ± 0.2 nS/pF (Glut+ODQ+cGMP, $n = 7$; $N = 3$). C) cGMP concentrations increased with glutamate stimulation, while the mGluR agonist tACPD did not. cGMP concentrations were 9.8 ± 0.3 nM (Ctrl, $n = 20$; $N = 6$), 10.8 ± 0.2 nM (Glut, $n = 10$; $N = 4$) and 9.6 ± 0.5 nM (tACPD, $n = 10$; $N = 4$). *, $p < 0.05$.

Endogenous or exogenous glutamate activates AMPARs that increase cytosolic cGMP and inhibit K_{ATP} channels. Inhibition of K_{ATP} then increases $[Ca^{2+}]_i$ to a limited level and promotes the docking of insulin-containing granules. When a high driving force occurs (depolarization or high glucose stimulation), exocytosis and insulin release are therefore increased.

Materials and Methods

All animal procedures were conducted in accordance with the National Institutes of Health Guide for the Care and Use of Laboratory Animals and all protocols were approved by the Animal Experimentation Ethics

Committees of Zhejiang University and Maribor University. Male mice at 8 to 10 weeks of age were used throughout the study. Kir6.2 knock-out mice were identified using the protocols reported previously (34). All drugs were from Sigma (St Louis, MO), Tocris (Bristol, UK) or Ascent Scientific (Bristol, UK) unless stated otherwise.

Pancreatic slice preparation

Pancreatic slices were prepared according to our previous work (16). In brief, the abdominal cavity of mice was opened and warm (37°C) low-gelling agarose (1.9% wt/vol; Seaplaque GTG agarose, BMA Products) was injected into the distally clamped bile duct. The whole pancreas was immediately cooled with ice-cold extracellular solution (ECS, in mM): 125 NaCl, 2.5 KCl, 26 NaHCO_3 , 1.25 NaH_2PO_4 , 2 Na-pyruvate, 0.5 ascorbic acid, 3 myo-inositol, 6 lactic acid, 1 MgCl_2 , and 2 CaCl_2 , adjusted to pH 7.3 and oxygenated with 95% O_2 /5% CO_2 , 300 ± 10 mOsm/kg. The pancreas

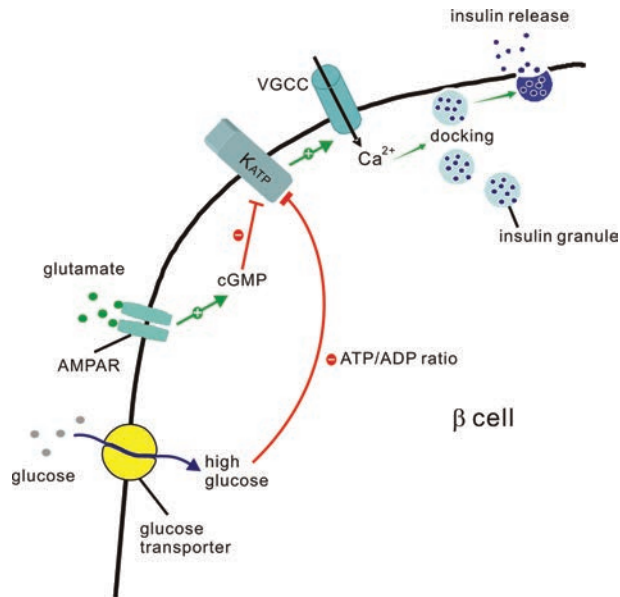


Figure 10: A proposed model. Schematic diagram showing how AMPARs act on exocytosis and insulin release in β cells. See Discussion for explanation.

in hardened agarose was extracted, placed in a small dish filled with warm agarose, and cooled rapidly on ice. Four small cubes were cut from the agarose-embedded pancreatic tissue and glued onto the sample plate of a vibrating tissue slicer (VT1000S, Leica, Wetzlar, Germany). Slices (140 μ m) were cut at 0.05 mm/seconds and 70 Hz in ice-cold ECS bubbled with 95% O_2 /5% CO_2 . Slices were kept in ice-cold ECS for at least 1 h before use.

Electrophysiology

Slices were placed in a submerged chamber and perfused with ECS (30°C) at 1.5 ml/min. Cells were visualized under an upright microscope (Nikon Eclipse E600FN, Nikon; Zeiss Axioskop 2 FS, Carl Zeiss) and a mounted CCD camera with 5 \times digital amplification (Cohu). β cells from the second or third layers in selected islets were used for whole-cell recording. The recording pipettes were pulled on an electrode puller (P-97, Sutter Instruments) and had resistances of 2–4 M Ω in CsCl-based solution. To measure glutamate currents, electrodes were filled with a solution containing (in mM) 125 CsCl, 40 HEPES, 2 MgCl₂, 20 tetraethylammonium-Cl (TEA-Cl) (pH 7.2 with CsOH). To measure voltage oscillation, K_{ATP} conductance and $[Ca^{2+}]_i$, electrodes were filled with a solution containing (in mM): 150 KCl, 10 HEPES, 2 MgCl₂, 0.05 EGTA (pH 7.2 with KOH) (16). ATPNa₂ was added in pipette solution according to the individual experiment. Whole-cell responses were filtered at 3 kHz and digitized at 10 kHz using either a SWAM IIC patch-clamp amplifier (Celica) or an EPC10 amplifier (HEKA). MPS-2 multichannel microperfusion (MPS-2, INBIO) was used to locally puff drug solutions onto cells. Each injector delivered solution at a flow rate of ~0.25 mL/min. The amplitude of the equilibrium response was the mean value of data points measured for the last 1 second before the termination of drug application.

Exocytosis detection

The capacitance change induced by single or train depolarization pulses (15,20,21) was used to measure the exocytosis of β cells. A 20-mV peak-to-peak 800 Hz sine wave was added to the holding potential by EPC-10 amplifier (HEKA) and 10 cycles were averaged for each data point. The extracellular solution contained (in mM): 118 NaCl, 20 TEA-Cl, 5.6 KCl, 1.2 MgCl₂, 5 HEPES (pH 7.4 with NaOH), 2.6 CaCl₂ and 5 D-glucose. The

pipette solution contained (in mM): 125 potassium glutamate, 10 KCl, 10 NaCl, 1 MgCl₂, 0.05 EGTA, 3 Mg-ATP, 0.1 cAMP and 5 HEPES (pH 7.1 using KOH) (20,21). All experiments were conducted at 32°C. To calculate the ΔC_m in train-stimulation experiments, the data points obtained over 12.5 milliseconds before the depolarization was averaged and set as the baseline value using Matlab (Math Works). The data points obtained over 500 milliseconds after depolarization was averaged and set as the C_m value.

Nested RT-PCR

After identification by electrophysiological characteristics, cell contents were harvested using glass micropipettes (OD 2 μ m) and placed in centrifuge tubes. The contents collected from five cells were then subjected to RT-PCR using a Qiagen OneStep RT-PCR Kit. The PCR primers used in this step are listed in Table S2. The second round of PCR after the RT-PCR was performed immediately. RT-PCR products were amplified by PCR using KOD plus polymerase (Novagen). The nested-PCR primers used are also listed in Table S2. Ten microliters of each nested-PCR product was placed on a 1.5% agarose gel and visualized by ethidium bromide staining. Nested-PCR products were further harvested and purified using NucleoSpin Extract II (Macherey-nagel) and sequenced by GenScript Corp.

Immunohistochemistry

Pancreatic immunohistochemistry was conducted according to previous reports (10,33,43,44). In brief, male C57 mice heart were perfused with physiological saline (0.9% NaCl) followed by 4% paraformaldehyde in phosphate-buffered saline (PBS) containing (in mM) 137 NaCl, 2.7 KCl, 1.5 KH₂PO₄, 10.1 Na₂HPO₄ (pH = 7.4). The pancreas was then removed and immersed in the same fixative for an additional 6 h. After fixation, the pancreatic tissues were placed in PBS containing 30% sucrose at 4°C until they sank, embedded in tissue-freezing medium (OCT compound), cryosectioned (35 μ m/section) and air-dried. Pancreas sections were blocked in 10% BSA/0.4% Triton/PBS solution (blocking serum) for 30 min at RT and immediately exposed to the primary antibodies for immunostaining overnight at 4°C. The primary antibodies used were rabbit monoclonal insulin antibody (1:400; Cell Signaling) and mouse monoclonal GluR2 antibody (1:500; Millipore). The sections were then rinsed in PBS and incubated with fluorochrome-conjugated secondary antibodies (Alex543, 1:1000; Alex488, 1:1000; Invitrogen) for 1 h at room temperature. Immunocytochemistry images were obtained with a confocal microscope (Olympus) at a resolution of 800 \times 800 pixels with the pinhole set at 1 airy unit. All the parameters used in confocal microscopy were consistent in each experiment. MetaMorph 5.0 software (Universal Imaging) was used to analyze the cell images.

Islet isolation and insulin secretion test

Non-fasting male mice (8 weeks) were euthanized by cervical dislocation and immediately the abdominal cavity was opened and collagenase (2 mg/mL dissolved in Hank's buffer; Roche) was injected into the pancreatic duct. The whole pancreas was extracted and digested for 25 min at 37°C and then washed with collagenase-free solution. Islets were individually selected under a microscope to ensure pure islet preparations and maintained (for <16 h) in RPMI-1640 containing 5 mM glucose and 10% (v/v) fetal calf serum at 37°C (15). For the insulin secretion test, aliquots of equal numbers of islets (30 islets/batch) were counted under a scaled microscope and incubated in culture medium at 37°C (45 min). Then, aliquots of islets were incubated in fresh media supplemented with either 5 mM or 16.7 mM glucose. A 15- μ L media from the control, glutamate or glutamate+CNQX group were taken at 1, 20 and 30 min for measuring the insulin levels using an ELISA kit (Mouse Insulin Elisa Kit, Crystal Chem).

Fluo-4 Ca²⁺ imaging

For β cell Ca^{2+} imaging, 80 μ M Fluo-4 (Invitrogen) was added to a K⁺-based internal saline. The dye was allowed to diffuse into cells for at least 2 min after the whole cell configuration was established. Ca^{2+} transients were elicited by local application of extracellular glutamate and recorded using a

laser scanning confocal microscope (LSM Exciter, Carl Zeiss). Fluo-4 was excited with the 488 nm line of an argon ion laser, and emitted light was collected through a 505-nm long-pass filter. Fluo-4 images were sampled in frame-scan mode at a frame rate of 1 Hz. For analysis, a region of interest that applied to all frames in a series of images was determined by manual thresholding foreground pixels, and these foreground pixels were then spatially averaged to calculate F for each frame (i.e. F is the fluorescence intensity at a timed point). The first 10 image frames in each experiment were averaged and used as the F_0 . Levels of $[Ca^{2+}]_i$ were expressed as F/F_0 ratios.

$[Ca^{2+}]_i$ measurements

$[Ca^{2+}]_i$ was measured according to our previous work (30). In brief, β cells were loaded with the K^+ salt of the leakage-resistant Ca^{2+} indicator Fura-PE3 (50 μM , added to the EGTA-free pipette solution; TEF Lab) in the patch pipettes. All cells were then exposed to monochromatic light (Polychrome IV, TILL Photonics) that alternated between 340 and 380 nm (50 Hz) and was filtered at 410 nm, reflected by a dichroic mirror (centered at 400 nm), and directed through a 60 \times water-immersion objective focused on the vertical midline section of the patched and loaded cell. The emitted fluorescence was transmitted by the dichroic mirror and further filtered through a 470-nm barrier filter. Images were obtained at 50 Hz (6-millisecond exposure time) using a cooled emCCD camera (Ixon, Andor Technology) and native Andor software. $[Ca^{2+}]_i$ was calculated from the background-subtracted intensity ratios of the images obtained with 340 and 380 nm excitation using the equation derived by Grynkiewicz et al. (45): $[Ca^{2+}]_i = K_d * [(F - F_{min}) / (F_{max} - F)]$, where K_d is the dissociation constant for Fura-PE3 of our experimental setup, F is the measured fluorescence intensity ratio, F_{max} and F_{min} are the ratios obtained by intracellular three-point *in vivo* calibrations with EGTA-buffered intracellular solutions containing no ($[Ca^{2+}]_{free} = 0 \mu M$; 10 mM K^+ -EGTA), a defined ($[Ca^{2+}]_{free} = 0.367 \mu M$; 3 mM K^+ -EGTA, 7 mM Ca^{2+} -EGTA), and a saturating concentration of free Ca^{2+} ($[Ca^{2+}]_{free} \approx 36 \mu M$, 10 mM Ca^{2+} -EGTA). Free Ca^{2+} was calculated using the Max-Chelator software (46). Three β cells were filled with each calibration solution and mean values of 1.2 μM , 0.14 and 0.98 for K_d , F_{min} and F_{max} were obtained. All necessary calculations were performed using a custom written Matlab script, and image acquisition and hardware triggering parameters were calculated and controlled by a custom AndorBasic (Andor Technology) program.

β -cell culture and transfection

β cells were cultured as in a previous report (47). In brief, collected islets were maintained at 37°C in RPMI-1640 containing 5 mM glucose and 10% (v/v) fetal calf serum before experiments. β cells were dispersed from islets treated with Dispase-II (0.3 mg/mL for 12 min), plated on glass coverslips pre-coated with poly-L-lysine and allowed to grow in RPMI-1640 supplemented with 10% (v/v) fetal bovine serum, 100 $\mu g/mL$ streptomycin, 100 IU/mL penicillin and 5 mM glucose at 37°C, and gassed with 95% O_2 /5% CO_2 . To observe the movement of insulin-containing granules, recombinant adenovirus adex1CA-insulin-eGFP plasmid, a gift from Dr Tao Xu (Institute of Biophysics, Chinese Academy of Sciences, China), was used to transfect β cells at DIV3 after dispersion. One hundred microliters of adex1CA-insulin-eGFP plasmid was added to cultured cells to a final volume of 2 mL for 6 h transfection that was terminated by washing with RPMI 1640. TIRFM experiments were performed in ECS 48 h after the transfection. Prior to the imaging experiments, β cells were transferred to a home-made closed perfusion chamber.

TIRFM imaging and analysis

The TIRFM observations were conducted in a previously described imaging setup located in the Institute of Biophysics, Chinese Academy of Sciences (Beijing, China) (24,48). The penetration depth of the evanescent field was estimated to be 113 nm by measuring the incidence angle with a prism ($n = 1.518$) and a 488-nm laser beam. Cells were transferred to a thermostat-controlled chamber (30°C) to avoid illumination damage (7).

Images were collected at 5 Hz using Cascade 650 (Roper Scientific) and imaging was controlled using Metamorph (Universal Imaging).

A semi-automated program in Matlab was used to analyze the insulin granules. Briefly, raw images were processed by a KNN filter (k-nearest neighbor) to restrain hotspot noise from the CCD. The images were further low-pass filtered at 0.5 Hz to remove high-frequency noise. Three hundred consecutive images (1 min) were collected for each drug perfusion (control, or glutamate, or glutamate+CNQX). To distinguish docking events, we measured radial fluorescence diffusion by manually placing two concentric circles centered on each vesicle being analyzed (Figure S2A). Identified particles were fitted with a 2D Gaussian function to obtain the peak location and width (24,48). Only particles with a width of Gaussian fit ≥ 200 nm and ≤ 666 nm were included for further analysis (Figure S2C). The Gaussian peak was taken as the lateral position. The relative axial position was calculated as $Z_n = -d \ln(F_n) / (F_{max})$, where F_n is the background-subtracted fluorescence in frame n , d is the penetration depth, and F_{max} is the maximum fluorescence intensity (49). We calculated the 3D displacement as $R^{(3)} = [(x_n - x_0)^2 + (y_n - y_0)^2 + (z_n - z_0)^2]^{1/2}$, where (x_n, y_n, z_n) stands for the position of the vesicle in frame n and (x_0, y_0, z_0) stands for the average position of the docking site. Two criteria were used to define a docked event: the fluorescence intensity in the inner circle exceeded three times the standard deviation of the background fluorescence (Figure S2A,B); and the vesicle remained immobile ($R^{(3)} < 0.067 \mu m$) during the observation (Figure 3B).

K_{ATP} channel conductance

K_{ATP} channel conductance ($G_{K_{ATP}}$) was measured according to previous work (28,17,33). Whole-cell patch-clamp with K^+ -based 0 ATP pipette solution was made to allow dialysis of intracellular ATP (28,33). After the whole-cell configuration, ramp stimuli (-100 mV to -40 mV at 0.6 mV/milliseconds steps) were applied at 1 Hz. The dominant current component between -100 and -40 mV ran through tolbutamide-sensitive K_{ATP} channels. At membrane potentials exceeding -30 mV, voltage-dependent K^+ channels were activated (17). Mean amplitudes of current in the first and last 10 milliseconds were acquired in an individual ramp. The increments of current between these two durations (ΔI) were calculated as the current values of the ramp. The increment of voltage between first and last 10 milliseconds (ΔV) was measured as 54 mV. The K_{ATP} channel conductance was thereby calculated by Ohm's law ($G_{K_{ATP}} = \Delta I / 54$ mV) and depicted as one data point.

cGMP assay

After identification by electrophysiological characteristics, cell contents were harvested using glass micropipettes (OD 2 μm) and quickly transferred to a centrifuge tube frozen in ice. The samples were analyzed with a mouse cGMP ELISA assay kit (Rapidbio) according to the instruction.

Data analysis

For electrophysiological recordings, cells were excluded from the study if series resistance varied by $>15\%$ over the course of the experiment. Offline analysis was done using Excel (Microsoft), LSM Examiner (Carl Zeiss), Image J (Wayne Rasband, NIH), SigmaPlot (Systat Software), MatLab and Igor Pro (WaveMetrics). Statistical differences were determined using either Student's *t*-test for two-group comparisons or one-way ANOVA with Tukey's test for multiple comparisons among more than two groups. Statistical significance was accepted at $p < 0.05$ (*) or $p < 0.01$ (**). Data in the text and figures are presented as mean \pm SEM.

Acknowledgments

We thank Drs Jin-Zhong Zhang and Tao Xu (Institute of Biophysics, Chinese Academy of Sciences, Beijing, China) for their help in TIRF experiments. We thank Dr Susumu Seino (Kobe University, Kobe, Japan) and Gang

Hu (Nanjing Medical University, Nanjing, China) for providing the Kir6.2 knock-out mice. We are grateful for helpful advice from Dr Li-Jun Kang and members of Shen lab. This work was supported by grants from National Basic Research Program (973) of the Ministry of Science and Technology of China (2009CB94140 and 2011CB5044000), National Foundation of Natural Science of China (30600168, 31070945, 30960108, 31060140 and 81170733), joint grant from National Foundation of Natural Science and Research Grants Council of Hong Kong, China (30731160616 and N_HKUST605/07), New Century Talent Award of the Ministry of Education of China (NCET-07-0751), Zhejiang Provincial Foundation of Natural Science (R206018) and joint grant from Chinese-Slovenian Scientific and Technological Cooperation. M. R. was supported by Slovenian Research Agency grant (J2-2290-2334) and Max-Planck International Partner Group Scheme. Z.-Y. W. was supported by an Ad-Futura travel grant. All authors declare that there are no conflicts of interest on this article.

Supporting Information

Additional Supporting Information may be found in the online version of this article:

Figure S1: CNQX inhibits exocytosis. Representative depolarization-evoked exocytosis responses from one β cell. The cell was voltage-clamped at -80 mV and then depolarized to 0 mV for 500 milliseconds to induce exocytosis (upper trace). The exocytosis tests were repeated in control (black) and with CNQX (blue). Membrane capacitance was calculated before and after depolarization. The responses during depolarization replaced by dashed lines. Note that CNQX perfusion decreased the exocytosis, as indicated by the bar graph. * $p < 0.05$.

Figure S2: Measurement of docked vesicles. A) TIRFM images of an insulin-eGFP vesicle docked on the plasma membrane. Times indicated are relative to the onset of docking. Gaussian fits of the radial fluorescence profile (in arbitrary units) of the vesicles are plotted below each image. Scale bar = $0.2 \mu\text{m}$. B) Time courses of the fluorescence intensity (FI) in arbitrary units (AU) in the inner circle and the annulus centered on the insulin-eGFP particle. The inner circle and the annulus are depicted in (A) with diameters of 0.4 and $0.55 \mu\text{m}$. C) Size distribution of 60 insulin-eGFP particles. The width of the Gaussian fit, δ , was used as a measure of size. The Y axis shows the number of vesicles and the line is the Gaussian fit of the distribution with a peak at 453 nm.

Figure S3: AMPAR effects are not mediated by neighboring cells. β cells were pre-treated and continuously perfused with $5 \mu\text{M}$ mefloquine. K_{ATP} channel conductance was measured by intracellular dialysis with 0 ATP in the pipette. Traces represent K_{ATP} channel conductance recorded in mefloquine (Meflo, black) and glutamate+mefloquine (Meflo+Glut, gray). Each conductance data point was acquired from one ramp (100 milliseconds) stimulation that was given at 1 Hz. Black triangles show the peak of each response. Statistics of normalized conductance is shown at right. The mean values of conductance were 3.7 ± 0.2 nS/pF (Meflo, $n = 5$; $N = 2$) and 2.9 ± 0.3 nS/pF (Meflo+Glut, $n = 10$; $N = 3$). *, $p < 0.05$.

Table S1: Alignment of DNA sequences

Table S2: PCR primers

Movies S1: This movie shows time-lapse TIRFM images of a single β cell in control. The cell was perfused with control solution (labeled at top left). This movie lasts for 16 seconds (AVI, 2.1 MB). The elapsed time points during imaging are labeled at top right. The fluorescent particles show insulin-containing granules. Selected frame is shown in Figure 3A. Scale bar: $3 \mu\text{m}$.

Movie S2: This movie shows time-lapse TIRFM images of a single β cell in glutamate. Same cell was perfused with glutamate-containing solution (labeled at top left). This movie lasts for 16 seconds (AVI, 2.1 MB). The elapsed time points during imaging are labeled at top right. The fluorescent particles show insulin-containing granules. Selected frame is shown in Figure 3A. Scale bar: $3 \mu\text{m}$.

Movie S3: This movie shows time-lapse TIRFM images of a single β cell in glutamate with CNQX. Same cell was perfused with glutamate+CNQX-containing solution (labeled at top left). This movie lasts for 16 seconds (AVI, 2.1 MB). The elapsed time points during imaging are labeled at top right. The fluorescent particles show insulin-containing granules. Selected frame is shown in Figure 3A. Scale bar: $3 \mu\text{m}$.

Please note: Wiley-Blackwell are not responsible for the content or functionality of any supporting materials supplied by the authors. Any queries (other than missing material) should be directed to the corresponding author for the article.

References

- Suckale J, Solimena M. The insulin secretory granule as a signaling hub. *Trends Endocrinol Metab* 2010;21:599–609.
- Sperling MA. ATP-sensitive potassium channels-neonatal diabetes mellitus and beyond. *N Engl J Med* 2006;355:507–510.
- Rorsman P, Eliasson L, Kanno T, Zhang Q, Gopel S. Electrophysiology of pancreatic β -cells in intact mouse islets of Langerhans. *Prog Biophys Mol Biol* 2011;107:224–235.
- Gonoi T, Mizuno N, Inagaki N, Kuromi H, Seino Y, Miyazaki J, Seino S. Functional neuronal ionotropic glutamate receptors are expressed in the non-neuronal cell line MIN6. *J Biol Chem* 1994;269:16989–16992.
- Muroyama A, Uehara S, Yatsushiro S, Echigo N, Morimoto R, Morita M, Hayashi M, Yamamoto A, Koh DS, Moriyama Y. A novel variant of ionotropic glutamate receptor regulates somatostatin secretion from delta-cells of islets of Langerhans. *Diabetes* 2004;53:1743–1753.
- Inagaki N, Kuromi H, Gonoi T, Okamoto Y, Ishida H, Seino Y, Kaneko T, Iwanaga T, Seino S. Expression and role of ionotropic glutamate receptors in pancreatic islet cells. *FASEB J* 1995;9:686–691.
- Yamada H, Otsuka M, Hayashi M, Nakatsuka S, Hamaguchi K, Yamamoto A, Moriyama Y. Ca^{2+} -dependent exocytosis of L-glutamate by αTC6 , clonal mouse pancreatic α cells. *Diabetes* 2001;50:1012–1020.
- Hayashi M, Yamada H, Uehara S, Morimoto R, Muroyama A, Yatsushiro S, Takeda J, Yamamoto A, Moriyama Y. Secretory granule-mediated co-secretion of L-glutamate and glucagon triggers glutamatergic signal transmission in islets of Langerhans. *J Biol Chem* 2003;278:1966–1974.
- Moriyama Y, Hayashi M. Glutamate-mediated signaling in the islets of Langerhans: a thread entangled. *Trends Pharmacol Sci* 2003;24:511–517.
- Weaver CD, Yao TL, Powers AC, Verdoorn TA. Differential expression of glutamate receptor subtypes in rat pancreatic islets. *J Biol Chem* 1996;271:12977–12984.
- Cabrera O, Jacques-Silva MC, Speier S, Yang SN, Köhler M, Machado A, Vieira E, Zierath JR, Kibbey R, Berman DM, Kenyon NS, Ricordi C, Caicedo A, Berggren PO. Glutamate is a positive autocrine signal for glucagon release. *Cell Metab* 2008;7:545–554.
- Cho JH, Chen L, Kim MH, Chow RH, Hille B, Koh DS. Characteristics and functions of α -amino-3-hydroxy-5-methyl-4-isoxazolepropionate receptors expressed in mouse pancreatic α -cells. *Endocrinology* 2010;151:1541–1550.
- Vignali S, Leiss V, Karl R, Hofmann F, Welling A. Characterization of voltage-dependent sodium and calcium channels in mouse pancreatic α - and β -cells. *J Physiol* 2006;572:691–706.
- Speier S, Gjinovci A, Charollais A, Meda P, Rupnik M. Cx36-mediated coupling reduces beta-cell heterogeneity, confines the stimulating glucose concentration range, and affects insulin release kinetics. *Diabetes* 2007;56:1078–1086.
- Göpel S, Kanno T, Barg S, Rorsman P. Patch-clamp characterisation of somatostatin-secreting δ cells in intact mouse pancreatic islets. *J Physiol* 2000;528:497–507.
- Speier S, Rupnik M. A novel approach to in situ characterization of pancreatic beta-cells. *Eur J Physiol* 2003;446:553–558.
- Ashcroft FM, Rorsman P. Electrophysiology of the pancreatic β -cell. *Prog Biophys Mol Biol* 1989;54:87–143.
- Hollmann M, Heinemann S. Cloned glutamate receptors. *Annu Rev Neurosci* 1994;17:31–108.

19. Giovannucci DR, Stuenkel EL. Regulation of secretory granule recruitment and exocytosis at rat neurohypophysial nerve endings. *J Physiol* 1997;498:735–751.
20. De Marinis YZ, Salehi A, Ward CE, Zhang Q, Abdulkader F, Bengtsson M, Braha O, Braun M, Ramracheya R, Amisten S, Habib AM, Moritoh Y, Zhang E, Reimann F, Rosengren AH, et al. GLP-1 inhibits and adrenaline stimulates glucagon release by differential modulation of N- and L-type Ca²⁺ channel-dependent exocytosis. *Cell Metab* 2010;11:543–553.
21. Kwan EP, Xie L, Sheu L, Ohtsuka T, Gaisano HY. Interaction between Munc13-1 and RIM is critical for glucagon-like peptide-1 mediated rescue of exocytotic defects in Munc13-1 deficient pancreatic beta-cells. *Diabetes* 2007;56:2579–2588.
22. Kasai K, Fujita T, Gomi H, Izumi T. Docking is not a prerequisite but a temporal constraint for fusion of secretory granules. *Traffic* 2008;9:1191–1203.
23. Yasuda T, Shibasaki T, Minami K, Takahashi H, Mizoguchi A, Uriu Y, Numata T, Mori Y, Miyazaki J, Miki T, Seino S. Rim2alpha determines docking and priming states in insulin granule exocytosis. *Cell Metab* 2010;12:117–129.
24. Bai L, Wang Y, Fan J, Chen Y, Ji W, Qu A, Xu P, James DE, Xu T. Dissecting multiple steps of GLUT4 trafficking and identifying the sites of insulin action. *Cell Metab* 2007;5:47–57.
25. Bratanova-Tochkova TK, Cheng H, Daniel S. Triggering and augmentation mechanisms, granule pools, and biphasic insulin secretion. *Diabetes* 2002;51:S83–S90.
26. Rorsman P, Renström E. Insulin granule dynamics in pancreatic beta cells. *Diabetologia* 2003;46:1029–1045.
27. Seino S, Iwanaga T, Nagashima K, Miki T. Diverse roles of K(ATP) channels learned from Kir6.2 genetically engineered mice. *Diabetes* 2000;49:311–318.
28. Speier S, Yang SB, Sroka K, Rose T, Rupnik M. KATP-channels in beta-cells in tissue slices are directly modulated by millimolar ATP. *Mol Cell Endocrinol* 2005;230:51–58.
29. Proks P, Ashcroft FM. Modeling K_{ATP} channel gating and its regulation. *Prog Biophys Mol Biol* 2009;99:7–19.
30. Rose T, Efendic S, Rupnik M. Ca²⁺-secretion coupling is impaired in diabetic Goto Kakizaki rats. *J Gen Physiol* 2007;129:493–508.
31. Henquin JC, Ishiyama N, Nenquin M, Ravier MA, Jonas JC. Signals and pools underlying biphasic insulin secretion. *Diabetes* 2002;51:S60–S67.
32. Izumi T, Kasai K, Gomi H. Secretory vesicle docking to the plasma membrane: molecular mechanism and functional significance. *Diabetes Obes Metab* 2007;2:109–117.
33. Huang YC, Rupnik M, Gaisano HY. Unperturbed islet α -cell function examined in mouse pancreas tissue slices. *J Physiol* 2011;589:395–408.
34. Miki T, Nagashima K, Tashiro F, Kotake K, Yoshitomi H, Tamamoto A, Gono T, Iwanaga T, Miyazaki J, Seino S. Defective insulin secretion and enhanced insulin action in KATP channel-deficient mice. *Proc Natl Acad Sci U S A* 1998;95:10402–10406.
35. Pusch M, Neher E. Rates of diffusional exchange between small cells and a measuring patch pipette. *Pflügers Arch* 1988;411:204–211.
36. Han J, Kim N, Kim E, Ho WK, Earm YE. Modulation of ATP-sensitive potassium channels by cGMP-dependent protein kinase in rabbit ventricular myocytes. *J Biol Chem* 2001;276:22140–22147.
37. Han J, Kim N, Joo H, Kim E, Earm YE. ATP-sensitive K(+) channel activation by nitric oxide and protein kinase G in rabbit ventricular myocytes. *Am J Physiol Heart Circ Physiol* 2002;283:H1545–H1554.
38. Baltrons MA, García A. AMPA receptors are coupled to the nitric oxide/cyclic GMP pathway in cerebellar astroglial cells. *Eur J Neurosci* 1997;9:2497–2501.
39. Ryder JW, Falcone JF, Manro JR, Svensson KA, Merchant KM. Pharmacological characterization of cGMP regulation by the biarylpropylsulfonamide class of positive, allosteric modulators of alpha-amino-3-hydroxy-5-methyl-4-isoxazolepropionic acid receptors. *J Pharmacol Exp Ther* 2006;319:293–298.
40. Schrammel A, Behrends S, Schmidt K, Koesling D, Mayer B. Characterization of 1H [1,2,4]oxadiazolo[4,3a]quinoxalinone as a heme-site inhibitor of nitric oxide-sensitive guanylyl cyclase. *Mol Pharmacol* 1996;50:1–5.
41. Henquin JC. Triggering and amplifying pathways of regulation of insulin secretion by glucose. *Diabetes* 2000;49:1751–1760.
42. Eliasson L, Abdulkader F, Rorsman P. Novel aspects of the molecular mechanisms controlling insulin secretion. *J Physiol* 2008;586:3313–3324.
43. Hayashi M, Otsuka M, Morimoto R, Hirota S, Yatsushiro S, Takeda J, Yamamoto A, Moriyama Y. Differentiation-associated Na⁺-dependent inorganic phosphate cotransporter (DNPI) is a vesicular glutamate transporter in endocrine glutamatergic systems. *J Biol Chem* 2001;276:43400–43406.
44. Poy MN, Hausser J, Trajkovski M, Braun M, Collins S, Rorsman P, Zavolan M, Stoffel M. miR-375 maintains normal pancreatic alpha- and beta-cell mass. *Proc Natl Acad Sci U S A* 2009;106:5813–5818.
45. Gryniewicz G, Poenie M, Tsien RY. A new generation of Ca²⁺ indicators with greatly improved fluorescence properties. *J Biol Chem* 1985;260:3440–3450.
46. Patton C, Thompson S, Epel D. Some precautions in using chelators to buffer metals in biological solutions. *Cell Calcium* 2004;35:427–431.
47. Ammälä C, Ashcroft F-M, Rorsman P. Calcium-independent potentiation of insulin release by cyclic AMP in single beta-cells. *Nature* 1993;363:356–358.
48. Li CH, Bai L, Li DD, Xia S, Xu T. Dynamic tracking and mobility analysis of single GLUT4 storage vesicle in live 3T3-L1 cells. *Cell Res* 2004;14:480–486.
49. Oheim M, Stühmer W. Tracking chromaffin granules on their way through the actin cortex. *Eur Biophys J* 2000;29:67–89.